RESEARCH ARTICLE

Magnetic Fe₃O₄/multi-walled carbon nanotubes materials for a highly efficient depletion of diclofenac by catalytic wet peroxideoxidation

Ysabel Huaccallo[1,2] · Silvia Álvarez-Torrellas[1] · María Pilar Marín[3,4] · María Victoria Gil[5] · Marcos Larriba[1] · Vicente Ismael Águeda[1] · Gabriel Ovejero[1] · Juan García[1] 📧

Abstract

The aim of this work is to synthesize a magnetic magnetite/multi-walled carbon nanotube (Fe_3O_4/MWCNT) catalyst by a method combining co-precipitation and hydrothermal treatments for the efficient removal of diclofenac (DCF) by catalytic wet peroxide oxidation (CWPO). The support (MWCNTs) shows a moderate-large surface area and good adsorption capacity, leading to the improvement of the magnetite (Fe_3O_4) dispersion on its surface. The response surface methodology (RSM) was applied in order to find out the effect of the reaction parameters on DCF removal, allowing to establish the optimum operating conditions ($T = 60$ °C, $[H_2O_2]_0 = 2.7$ mM, [catalyst] = 1.0 g L^{-1}). The optimum CWPO experiment showed an outstanding catalytic activity at non-modified pH solution (6.7), obtaining a 95% of DCF removal after 3 h reaction time; this high efficiency can be attributed to the synergistic effect of the iron-based catalyst with the high quantity of $^\bullet$OH radicals generated on the surface of the catalyst. In addition, the Fe_3O_4/MWCNT material exhibited good reusability along three consecutive reaction cycles, finding a pollutant removal close to 95% in each cycle of 3 h reaction time. Additionally, a degradation mechanism pathway was proposed for the removal of DCF by CWPO. The versatility of the material was finally demonstrated in the treatment of different environmentally relevant aqueous matrices (a wastewater treatment plant effluent, surface water, and hospital wastewater), obtaining an effective reduction in the ecotoxicity values.

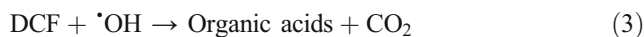Responsible editor: Vítor Pais Vilar

📧 Juan García
jgarciar@ucm.es

1 Catalysis and Separation Processes Group, Chemical Engineering and Materials Department, Chemistry Sciences Faculty, Complutense University, Avda. Complutense s/n, 28040 Madrid, Spain

2 Chemical Engineering Department, National University of Saint Agustine, Av. Independencia s/n, Arequipa, Peru

3 Departamento de Física de Materiales, Physical Sciences Faculty, Complutense University, Avda. Complutense s/n, 28040 Madrid, Spain

4 Applied Magnetism Institute, UCM-ADIF-CSIC, 28230 Las Rozas, Madrid, Spain

5 Departmento Química Orgánica e Inorgánica, Extremadura University, Avda. de Elvas, s/n, 06071 Badajoz, Spain

Introduction

Pharmaceutical compounds are a class of emerging environmental contaminants of high concern, due to their inherent capacity to induce adverse physiological effects in humans and wildlife even at very low doses (Ebele et al. 2017; Fischer et al. 2017). Among them, the non-steroidal anti-inflammatory drugs (NSAIDs) are one of the most widely used classes of drugs by humans and animals due to their analgesic, antipyretic, and anti-inflammatory properties. As it has been found in the literature, these pollutants possess the ability of disrupting the endocrine system, affecting the synthesis, secretion, transport, action, or elimination of natural hormones inside the body (Verlicchi et al. 2012; Rimayi et al. 2018). One of the most consumed NSAID compounds is diclofenac (DCF) and, consequently, it is one of the most frequently detected pollutants in the wastewater treatment plant (WWTP) effluents, with an absolute concentration which can reach up to the microgram per liter range (Verlicchi et al. 2012). So, in this work, DCF has been selected

due to its presence in many kinds of water environments (Luo et al. 2014; Ashfaq et al. 2017), such as influent wastewater and hospital wastewater effluents at significant concentrations (< 0.1 μg L^{-1} to 0.20 mg L^{-1}). In this sense, it has been estimated that the average DCF removal achieved in the conventional WWTPs is only between 21% and 40% (Chong et al. 2017). Due to its continuous and intensive input into the aquatic environment, its effects on living organisms have been widely studied. Besides the well-known toxic effects of DCF towards the vulture population reported by Oaks et al. (Oaks et al. 2004), renal and hepatic toxicity has also been recorded in certain fish species at concentrations in the low microgram per liter range (Ebele et al. 2017). For this reason, in the first review of the list of priority substances of the European Water Framework Directive (WFD), the Commission legislative proposal included an environmental quality standard (EQS) for DCF presence in the aquatic environment.

Commonly, the attention received by the conventional biological treatments far exceeds that of other treatment techniques, due to their low cost, high durability, and easy operation. Nevertheless, the behavior of the toxic and biorecalcitrant organic compounds along the process detracts the viability of the biological treatments (Benítez et al. 2011; Zupanc et al. 2013). In this context, the advanced oxidation processes (AOPs) have been reported as particularly efficient technologies for the removal of refractory organic pollutants, traceable organic contaminants or even some inorganic pollutants, or in particular cases to increase the wastewater biodegradability as a pre-treatment of a subsequent biological treatment stage. Generally, in the AOPs, powerful reactive hydroxyl ($^{\bullet}OH$) or sulfate ($SO_4^{\bullet -}$) radicals are produced by specific chemical reactions that occurred in aqueous solution (Deng and Zhao 2015; Chen et al. 2018). The reactive species ($^{\bullet}OH$ or $SO_4^{\bullet -}$) are able to degrade even the most recalcitrant organic molecules and convert them into less persistent and non-contaminant compounds, specifically short-chain organic acids (Do et al. 2018). In general terms, the heterogeneous Fenton reaction is an advanced oxidation process considered as catalytic wet peroxide oxidation (CWPO) that acts by generating highly reactive $^{\bullet}OH$ species due to the combination of Fe^{2+}, Fe^{3+}, and H_2O_2 in aqueous solution (Yu et al. 2015). In this process, Fe^{2+} ions are oxidized by H_2O_2 to Fe^{3+} and then one equivalent $^{\bullet}OH$ radical is generated (Ma et al. 2015). A reasonable mechanism of CWPO reaction with Fe_3O_4 supported on multi-walled carbon nanotube (MWCNT) catalyst can be proposed as follows:

$$Fe_3O_4/MWCNTs\left(Fe^{2+}\right)$$
$$+ H_2O_2 \rightarrow Fe_3O_4/MWCNTs\left(Fe^{3+}\right) + {}^{\bullet}OH + {}^{-}OH \quad (1)$$

$$Fe_3O_4/MWCNTs\left(Fe^{3+}\right)$$
$$+ H_2O_2 \rightarrow Fe_3O_4/MWCNTs\left(Fe^{2+}\right) + H^+ + {}^{\bullet}HO_2 \quad (2)$$

$$DCF + {}^{\bullet}OH \rightarrow Organic\ acids + CO_2 \quad (3)$$

$$Organic\quad acids + {}^{\bullet}OH \rightarrow CO_2 + H_2O \quad (4)$$

Some authors have reported fast and effective degradation of DCF while applying different AOP processes. The removal efficiency of diclofenac and reaction time used in the reported AOP techniques have been collected in Table 1 (Hofmann et al. 2007; Sklari et al. 2015; Chong et al. 2017; Gao et al. 2017; Zhang et al. 2017; Zhou et al. 2018).

On the other hand, carbon nanotubes (CNTs), including single-walled (SWCNTs) and MWCNTs, have been extensively investigated and used as catalytic supports, due to their excellent properties, such as moderate-high specific surface area and electronic conductivity (Ovejero et al. 2006; Das et al. 2014; Krstic et al. 2018). Indeed, several studies have demonstrated that the surface of the carbon nanotubes can be chemically functionalized to potentially enhance the density of active sites responsible for the $^{\bullet}OH$ generation, promoting the $^{\bullet}OH$ species formation (Garcia et al. 2006; Pinho et al. 2015). Moreover, the processes with carbon nanotubes acting as catalytic support generate a minimum leaching of the active phase, allowing to work at a wider pH range (Garcia et al. 2006; Ma et al. 2015). In addition, carbon nanotubes are also known to be relatively stable in extreme environments, maintaining their mechanical properties along the reaction.

Because the suspended catalysts are more effective in the degradation of pollutants compared to those immobilized on carriers, the solids need to be separated and recovered after the treatment. For this reason, it is necessary to explore new materials with good catalytic properties and high ability to be recovered from the reaction medium. In this context, magnetic catalysts have appeared as an effective alternative, since the catalyst can be easily separated from the aqueous solution by using an external magnetic field (Munoz et al. 2017; Ribeiro et al. 2017). In this sense, magnetite (Fe_3O_4) has been selected in this study to be incorporated onto the surface of commercial multi-walled carbon nanotubes in order to obtain a hybrid magnetic material that can be easily recovered from the reaction medium. The synthesis of the catalyst ($Fe_3O_4/MWCNTs$) was assessed following the combination of both co-precipitation and hydrothermal methods previously reported (Yu et al. 2015; Sharma et al. 2016). To the best of the authors' knowledge, this is the first work that based on the use of a synthesized magnetic material supported on carbon nanotubes for the removal of the emerging contaminant diclofenac from aqueous solution by CWPO reactions.

Herein, the authors firstly followed a facile synthesis route based on the incorporation of magnetite on the surface of the multi-walled carbon nanotubes. The morphological structure of the material was studied by transmission electron microscopy (TEM) technique. In addition, the textural and surface chemical properties of the catalyst were fully explored. The synthesized material showed good magnetic properties, an

Table 1 Comparison of iron-based catalytic systems for the removal of DCF in aqueous solution

Treatment process	Experimental conditions	Initial concentration (mg L^{-1})	Removal efficiency (%), time (min)	Reference
Heterogeneous Fenton	Fe-03 sphere commercial catalyst; 60 °C, [catalyst] = 5 g L^{-1}; 2.5 mL perhydrol	20.0	(40) (120)	Hofmann et al. (2007)
Electro-Fenton	Iron-impregnated carbon felts as cathodic electrodes; flow rate = 50 mL min^{-1}; 25 °C; pH 7; [Na$_2$SO$_4$] = 0.05 M	30.3	(44.6) (1600)	Sklari et al. (2015)
Catalytic ozonation	Iron silicate-loaded pumice; 25 °C	29.6	(73.3) (60)	Gao et al. (2017)
Heterogeneous Fenton	FeCeOx; pH 5.0; [H$_2$O$_2$]$_0$ = 3.0 mM; [catalyst] = 0.5 g L^{-1}; 25 °C	20.7	(84) (40)	Chong et al. (2017)
Heterogeneous sonocatalytic	N-Fe/AC; 325 W at 24 kHz	20.0	(100) (30)	Zhang et al. (2017)
ZVI/EDTA	[catalyst] = 0.4 g L^{-1}; 2 mM EDTA; 25 °C; pH 5	10.0	(90) (120)	Zhou et al. (2018)

excellent catalytic activity, and an outstanding recyclability at different rounds for DCF removal. The effect of the catalyst load, H_2O_2 dose, and temperature on the pollutant efficiency removal was evaluated by using the response surface methodology (RSM): Box-Behnken design (BBD), determining the optimal experimental conditions. Furthermore, the versatility of the catalyst was evidenced by their ability to efficiently remove the organic matter present in different environmentally relevant aqueous matrices.

Materials and methods

Materials

The commercial MWCNTs (diameter of 30–50 nm, length of 20 mm) were supplied by Sun Nanotech Co. Ltd. (Beijing, China). $FeCl_3 \cdot 6H_2O$, $FeCl_2 \cdot 4H_2O$, Na_2SO_3, ammonium hydroxide solution (28–30% w/w), and H_2O_2 solution (30% w/w) were purchased from Sigma-Aldrich (Belgium). Diclofenac as sodium salt, with a purity of more than 98%, was obtained from Sigma-Aldrich (Belgium). All the solutions used in the experiments were prepared in ultrapure water.

Synthesis of the catalyst

The synthesis of the catalyst was accomplished in two stages.

Functionalization of multi-walled carbon nanotubes

The purification and subsequent functionalization of the MWCNT surface were carried out in order to obtain a homogeneous deposition of the magnetite over the external walls of the support. Briefly, 2.0 g of MWCNTs was added to 200 mL of H_2O_2 solution (18% w/w). The MWCNTs/H_2O_2 suspension was heated at 80 °C for 4 h. Then, the solids were thoroughly washed with ultrapure water until the washing water reached neutral pH. The obtained MWCNTs were dried in an oven at 100 °C for 10 h (Ovejero et al. 2007).

Preparation of the catalyst

Fe_3O_4/MWCNT catalyst was prepared adapting the method previously reported by Yu et al. (Yu et al. 2015): (i) 0.20 g of the functionalized MWCNTs was added to 120 mL of ultrapure water at 60 °C and vigorously stirred in a three-neck flask under the purge of nitrogen gas; (ii) 0.28 g of $FeCl_3 \cdot 6H_2O$ and 0.08 g of $FeCl_2 \cdot 4H_2O$ and 0.5 mL of ammonia solution were added; (iii) the mixture was vigorously stirred at 60 °C under the purge of nitrogen gas for 30 min, forming a colloidal solution; (iv) the obtained colloidal solution was then transferred into a 180-mL Teflon-lined autoclave reactor (the autoclave was sealed and kept at 120 °C for 15 h and then naturally cooled to room temperature); (v) the precipitate was separated from the suspension by a magnet and then thoroughly washed with ultrapure water until the washing water reached a pH value of 6.7; and (vi) after repeated washing with ultrapure water under ultrasonication for 5 min, the obtained magnetic material was dried in a vacuum oven at 60 °C for 24 h. The obtained catalyst was labeled as Fe_3O_4/MWCNTs. The yield of Fe_3O_4/MWCNTs catalyst was 85.7% per batch.

Support and catalyst characterization

The morphology of the catalyst and the distribution of the magnetic nanoparticles supported on the MWCNTs were studied by using a TEM (JEOL 3000F). The thermogravimetric analyses (TGA) were carried out in a thermal analyzer TGA Q500 (STA 6000) under air flow, following a heating rate of 10 °C min^{-1} from 30 to 1000 °C. The crystalline phase of the samples was analyzed by X-ray diffraction (XRD, X' Pert MPD) with Cu Kα radiation ($\lambda = 1.5406$ Å). Thus, the porosity of the materials was measured by N$_2$ adsorption-desorption isotherms at 77 K in an ASAP 2020 apparatus, with the samples outgassed at 250 °C for 3 h before the measurement. The specific surface area of the solids (S_{BET}) was calculated using the Brunauer-Emmett-Teller (BET) equation and the micropore volume (V_{Mic}) was estimated by using Dubinin-Radushkevich equation. The Fourier-transform infrared spectra were recorded in a Thermo Nicolet FT-IR spectrophotometer, in a wavelength range from 400 to 4000 cm^{-1}. The elemental microanalysis was accomplished in a LECO CHNS-932 analyzer, where 0.6–1.6 mg of sample was held in a furnace at 1000 °C, where the combustion of the material occurred. Raman spectra were recorded in an Ntegra Spectra (NT-MDT) micro-Raman apparatus, equipped with a CCD Andor iDus detector. Finally, the magnetization curves of the Fe$_3$O$_4$/MWCNTs catalyst were measured using a MPMS-5S SQUID magnetometer from Quantum Design (San Diego, CA, USA). The total iron content in the solid samples was measured by wavelength dispersive X-ray fluorescence analysis (WDXRF), using an Aχios spectrometer (PANalytical) equipped with an Rh anode X-ray tube and a maximum power of 4 kW.

Catalytic activity evaluation

Batch CWPO experiments were conducted in a three-necked round-bottom glass flask (250 mL) with screw caps and equipped with a reflux condenser. The tests were accomplished under continuous stirring (700 rpm) at a constant temperature with a thermostatic bath. The reaction medium was prepared by adding the Fe$_3$O$_4$/MWCNT catalyst to a solution (130 mL) containing DCF as model pollutant with an initial concentration of 10.0 mg L^{-1}; then, the reaction was started with the addition of the required H$_2$O$_2$ dose. Each test in the experimental design (Table 2) was carried out at a solution pH of 6.7 (natural pH of DCF in ultrapure water) in order to minimize any contribution of homogeneous reaction (due to the possible leaching of the active phase). The experiments of recycling were carried out in the same way. After each reaction cycle, the stirring was stopped and the catalyst and treated effluent were separated by using a magnet. The treated effluent was collected and the catalyst was washed three times with

ultrapure water; after that, DCF solution and H$_2$O$_2$ were freshly added. Three reaction cycles were conducted in total.

At regular time intervals, samples were collected from the reactor after the magnetic separation of the catalyst and then filtered through PTFE syringe filters (0.45 μm) and immediately analyzed. It is noteworthy to say that the reaction was stopped by the addition of sodium sulfite before the analysis of the pollutant, in order to avoid the degradation of the drug after sample was taken from the reaction medium.

The data shown in Table 2 are the evaluated operating parameters in each experiment, e.g., temperature, catalyst, and H$_2$O$_2$ doses. Additionally, several blank experiments were considered in order to discard DCF removal by adsorption over the catalyst or oxidation via only hydrogen peroxide or catalytic homogeneous oxidation by the dissolved iron species. These experiments were conducted at 70 °C and pH of 6.7 using the support and the catalyst in the absence of the oxidant (adsorption tests), only with hydrogen peroxide (2.7 mM) in the absence of the catalyst (H$_2$O$_2$ test), and using hydrogen peroxide (2.7 mM) and a solution of 10.0 mg·L^{-1} of dissolved Fe^{2+} ions (homogeneous Fenton test).

DCF removal optimization by response surface methodology: Box-Behnken design

RSM was applied to evaluate the individual and interactive effects of the independent variables temperature, catalyst dosage, and H$_2$O$_2$ dose on the DCF removal (Ferreira et al. 2007; Khan et al. 2017). The range of each individual variable was determined based on the preliminary tests. The experiments were carried out at a pH of 6.7 and 10.0 mg L^{-1} as initial DCF concentration, in order to cover the range of 0–10.0 mg L^{-1} that could be found in real influents.

The performance of the CWPO process was optimized by BBD, using a second-order polynomial model (Eq. 5). The used coded levels in BBD can be seen in Table S1 (Supplementary Material). Thus, RSM methodology was applied to the experimental data using the commercial software Minitab (Ayazi et al. 2016). The theoretical optimized values could be compared to the experimental data.

In this study, only 15 experiments were needed including three replicates (see Table 2), but 27 experiments were carried out in order to explore the applicability of the obtained quadratic polynomial equation obtained.

The mathematical relationship between the independent factors and the response was established by fitting the experimental data to a quadratic polynomial equation, as expressed by Eq. 5:

$$\gamma = \beta_0 + \sum_{i=1}^{j} \beta_i x_i + \sum_{i=2}^{k} \beta_{ii} x_i^2 + \sum_i^{i<j} \sum_j \beta_{ij} x_i x_j \qquad (5)$$

where γ is the DCF removal percentage (%), x_i, x_j…x_k are the individual factors, x_i^2, x_j^2,…x_k^2 are the squared effects, $x_i x_j$,

Table 2 Experimental design matrix results of DCF degradation by CWPO

Run	Actual values			DCF removal efficiency (%)		
	A (H_2O_2 dosage) (mM)	B (catalyst dosage) (g L^{-1})	C (temperature) (°C)	Observed	Predicted	Error
1	1.00	0.50	50	52.9	49.6	3.3
2	1.00	0.75	40	58.6	57.6	− 1.0
3	1.00	0.75	50	53.1	52.5	0.6
4	1.00	0.75	60	61.7	66.8	− 5.1
5	1.00	1.00	50	70.1	69.9	0.2
6	1.85	0.75	50	53.0	53.5	− 0.5
7	1.85	1.00	40	73.6	76.1	− 2.5
8	1.85	1.00	60	88.2	85.3	2.9
9	2.70	0.50	50	59.2	62.3	− 3.1
10	2.70	0.50	60	76.4	76.6	− 0.2
11	2.70	0.75	40	71.8	70.3	1.5
12	2.70	0.75	60	82.0	79.5	2.5
13	2.70	1.00	50	82.0	82.6	− 0.6
14	1.85	0.75	50	53.2	53.5	− 0.3
15	1.85	0.75	50	54.0	53.5	0.5

Reaction conditions: $[DCF]_0 = 10.0$ mg L^{-1}, [catalyst] = 1.0 g L^{-1}, atmospheric pressure, 3 h reaction time

$x_i x_k$, and $x_j x_k$ are the interaction relationship between each individual factor, β_0 is a constant coefficient, and β_i, β_{ii}, and β_{ij} ($i = 1, 2,…, k$; $j = 1, 2,… k$) are the linear, quadratic, and interactive effects coefficients, respectively.

Furthermore, the effect of temperature (40, 50, and 60 °C) on the CWPO reaction at initial reaction conditions of 2.7 mM of H_2O_2, 1.0 g L^{-1} of catalyst, and pH of 6.7 was studied, in order to determine the reaction kinetics and the activation energy of DCF removal.

Analytical methods

DCF concentration was followed by high performance liquid chromatography, HPLC-UV/Vis (Varian, ProStar), using a PerkinElmer column (250 × 4.6 mm i.d., 5 μm). The analyses were performed at 274 nm using 50/50 (%, v/v) mixtures of acetonitrile and acidified water solution (0.1% w/w H_3PO_4) as mobile phase (0.5 mL min^{-1}) and a loop volume of 20 μL.

H_2O_2 concentration was measured in a UV-Vis spectrophotometer (Lambda 35, PerkinElmer) at a wavelength of 410 nm after adding a titanium (IV) oxysulfate solution and a yellow complex was formed. The calibration curve of the H_2O_2 concentration and the absorbance (Fig. S1 of the Supplementary Material) showed a linear plot through the origin, where Beer's law was fulfilled in the range 0.05–7.0 mM of H_2O_2 concentration. The iron that leached to the reaction medium was measured following the o-phenanthroline method (Munoz et al. 2017); in this case, the measurements were accomplished at a wavelength of 510 nm using a UV-Vis spectrophotometer (Lambda 35, PerkinElmer). Finally, the

raw real aqueous matrices were characterized by the determination of the total organic carbon (TOC) and total nitrogen (TN) concentrations using a TOC analyzer (Shimadzu TOC V_{SCH}), and the chemical oxygen demand (COD), conductivity, suspended solid concentration, aromaticity, phenolic compounds, and ammonium (NH_4^+) and nitrate (NO_3^-) concentrations were measured according to the Standard Methods (2005).

Identification of DCF transformation products

A sample of the DCF effluent was treated by dispersive liquid-liquid microextraction, following the procedure reported by Zgola-Grzeskowiak and Grzeskowiak (2010). Briefly, 6 mL of sample was adjusted to pH 1, and then, 1 mL of acetone containing 80 μL of chloroform was added rapidly into the sample solution. Fine drops were formed and sedimented in the bottom of the test tube. The sediment phase was withdrawn and the extract was dried with gentle pure nitrogen flow and injected into a liquid chromatograph (LC 1100, Agilent Technologies, Palo Alto, CA) coupled to a discovery ion trap mass spectrometer (HCT-Ultra PTM, Bruker, Bremen, Germany). The ESI ion source was operated at negative ion mode for all the analytes. DCF standard was also analyzed in order to compare with the DCF sample analyzed.

Toxicity assays

The change in the toxicity caused by CWPO treatment of real wastewaters was assessed by an internationally standardized

aquatic ecotoxicity test (Microtox M500 analyzer). The inhibitory effect of water samples on the light emission of the marine bacterium *Vibrio fischeri* was determined (luminescent bacteria test with Biotox testing kit; ISO 11348-3, 2009). The procedure of the analysis follows the standard procedure for Microtox® analysis (Álvarez-Torrellas et al. 2017). Bioluminescence was measured after 5 and 15 min exposure to the test solution. The test was carried out at 15 °C, adjusting the osmotic pressure close to 2% NaCl and pH between 6 and 8. The toxicity of each sample was defined as the percent of the inhibition of the luminescence relative to a noncontaminated blank (ultrapure water). When the relative inhibition percentage was found above 20%, the EC50 was calculated and subsequently converted in toxicity units (TUs).

Results and discussion

Catalyst characterization

TEM analyses were used in order to reveal the morphological properties of the catalyst. Figure 1. displays the TEM micrographs of the support (MWCNTs), the fresh catalyst (Fe_3O_4/MWCNTs), and the reused catalysts. Figure 1a, b showed the TEM images of MWCNT support after the functionalization. It could be observed that after being treated with H_2O_2, the multi-walled carbon nanotubes were open-ended and separated with relatively short length diameter. The treatment endowed the Fe_3O_4/MWCNTs catalyst with structural integrity and regular dispersion (Fig. 1c, d). The images of Fe_3O_4/MWCNT catalyst showed aggregates of many tiny Fe_3O_4 nanoparticles with spherical-like shape in the form of clusters on the surface of MWCNTs, with an average particle size about 4–11 nm. No changes in the morphology of the catalyst were observed after the first (Fig. 1e, f) and second reuse (Fig. 1g, h), where the magnetic particles maintain their spherical shape. This fact confirms the applicability of the synthesis method. The particle size of the catalyst used in the CWPO experiments was lower than 100 μm (Fig. 1).

TGA profiles of MWCNTs (a), Fe_3O_4 (c), and Fe_3O_4/MWCNT (b) materials are shown in Fig. 2. The weight loss at temperature lower than 100 °C was due to the evaporation of the water entrapped in the structure of the solid. The weight loss at temperature higher than 400 °C for the catalyst was lower than that observed for the support, attributed to the oxidation of the oxygenated groups on the surface of MWCNTs. Furthermore, Fe_3O_4 was transformed to Fe_2O_3 during the heat treatment, suggesting that the remaining 20% of ash corresponds to Fe_2O_3 as the product of oxidation of the magnetite. This fact demonstrated that Fe_3O_4 has been deposited on the support, in agreement to those observed in TEM micrographs (Ribeiro et al. 2017).

The temperatures of maximum weight loss (T_{max}) were obtained of approximately 564 and 608 °C, for all the magnetic materials and the support, respectively (Fig. 2). This difference between both values indicated that the presence of iron oxides in the catalyst had a main influence on the thermal stability of the materials (Buzarovska et al. 2015).

The structure phase of the catalytic support and the prepared catalyst was analyzed by using XRD patterns of the powdered samples (Fig. 3a). The peaks at 2 = 29.7, 35.2, 43.1, 57.1, and 62.7 were attributed to (220), (311), (400), (511), and (440) crystal planes of face-centered cubic (FCC) of Fe_3O_4, respectively, in accordance with the standard XRD pattern of Fe_3O_4 (Wang et al. 2014). The XRD patterns of the reused catalysts after the first and second cycles are shown in Fig. 3b. As it can be seen, the XRD results did not reveal any phase transformation, supporting the stability of the catalyst in CWPO process, showing a promising service lifetime and potential in wastewater treatment practical applications.

The surface functionalities of the prepared magnetic catalyst were investigated by the spectroscopic results from FT-IR studies (Fig. 3c), which were carried out for a better comprehension of the structure and composition of the materials. An absorption band revealing the vibrational properties of the Fe-O bond was observed around 586 cm^{-1} in the FT-IR catalyst spectrum. This band is mainly assigned to the stretching vibrations of Fe-O-Fe. The broad absorption peaks found between 3400 and 3500 cm^{-1} correspond to –OH groups, attributed to the presence of hydroxyl groups on the surface of the composite or the adsorption of some atmospheric water during FT-IR measurements. The band at 1621 cm^{-1} can be assigned to the C=O stretching mode of the functional groups on the surface of the MWCNTs. Thus, the peak at 2940 cm^{-1} observed in the FT-IR spectrum of the support is characteristic of the C– stretch vibration in the surface of MWCNTs (Li et al. 2016).

N_2 adsorption-desorption isotherms at 77 K of the materials are shown in Fig. 3d, since the estimated textural properties (specific surface area, S_{BET}, micropore volume, V_{Mic}, total pore volume, V_{Total}, and average pore width) of the MWCNTs and Fe_3O_4/MWCNTs catalyst have been reported in Table S2 (Supplementary Material). The BET surface area values of the support and the catalyst, estimated by the Brunauer-Emmett-Teller equation, were found very similar (97 and 90 m^2 g^{-1}, respectively), indicating that the incorporation of magnetite in the support did not change the textural properties. In general terms, it could be concluded that the materials are essentially mesoporous (type IVa isotherms), with very low micropore volume values (0.06 and 0.05 cm^3 g^{-1}), for the support and the catalyst, respectively, and average pore widths of 17.9 and 14.9 nm, confirming the mesoporosity of the materials (Álvarez-Torrellas et al. 2018).

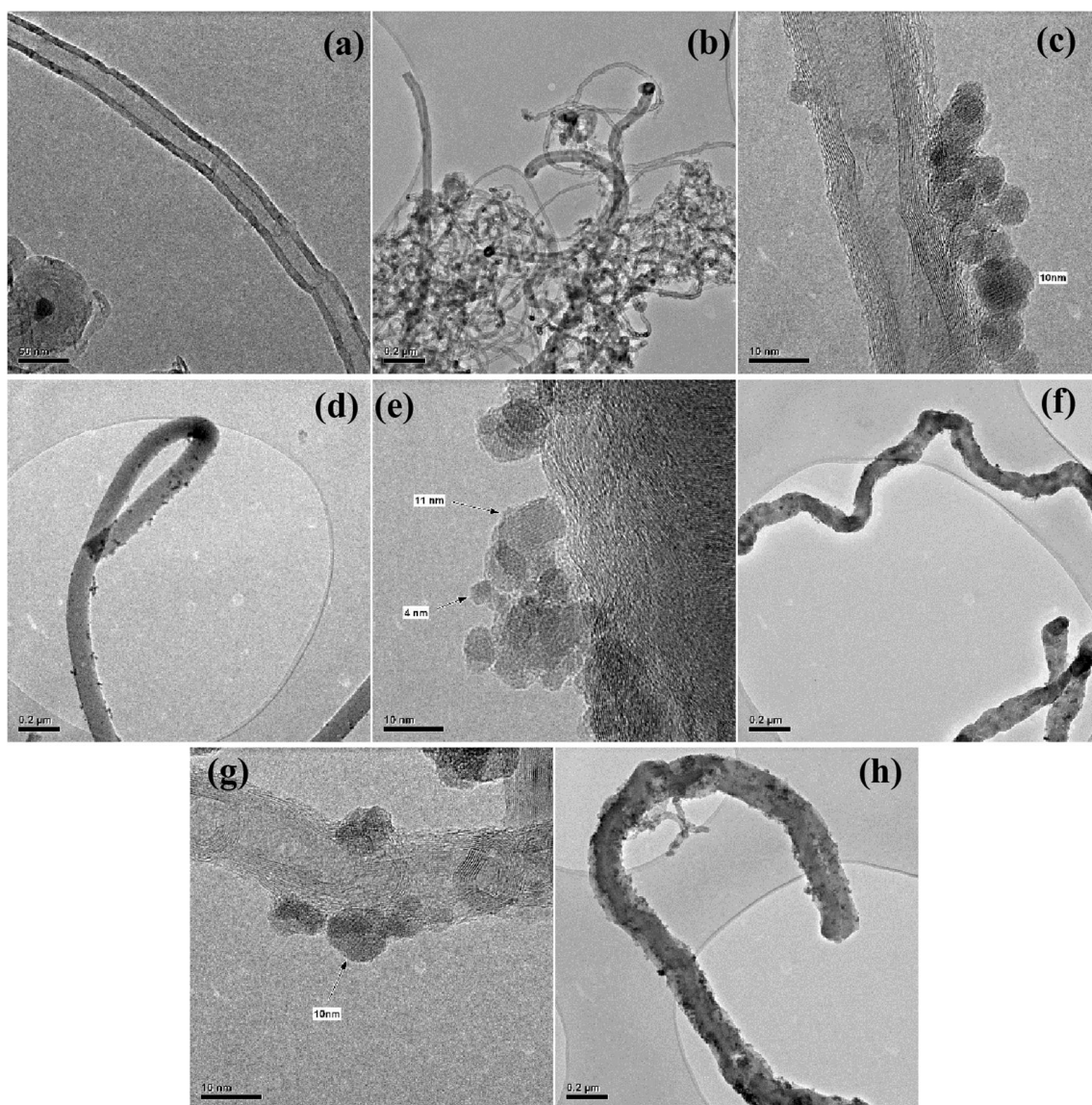The elemental analysis of the functionalized MWCNTs, fresh Fe_3O_4/MWCNTs, and the reused Fe_3O_4/MWCNTs

Fig. 1 TEM micrographs of (a, b) MWCNTs, (c, d) Fe₃O₄/MWCNTs, (e, f) Fe₃O₄/MWCNTs-1 (first reused) and (g, h) Fe₃O₄/MWCNTs-2 (second reused)

catalysts is collected in Table 3. Thus, the carbon percentage (%C) measured in MWCNTs and fresh and reused catalysts (Fe₃O₄/MWCNTs-1 and Fe₃O₄/MWCNTs-2) was 84.47%, 57.99%, 54.07%, and 54.27%, respectively. Compared to that found in the fresh catalyst, the %C measured in the second- and third-reused catalysts were similar, indicating that the formation of carbonaceous deposits on the catalyst surface did not occur after the CWPO process.

The measurements of total iron of the solids, e.g., the fresh and reused catalysts, were carried out by WDXRF, finding values of 21.36, 22.77, and 15.18 mg, respectively (Table 3). The difference observed in the iron content of the second and third-reused catalysts can be attributed to the non-well dispersion of the active phase on the catalytic support. This can be assessed by the agglomeration of magnetite observed in some

areas of the surface support, as it can be seen in TEM micrographs (Fig. 1c–f).

Furthermore, the iron concentration of the CWPO effluents with the second- and third-reused catalysts was evaluated by o-phenanthroline method, obtaining a value of leached iron of 0.1 mg L^{-1}, for both samples. The low iron content in the effluents can be considered as negligible, attending to the low solubility of Fe^{+3} and Fe^{+2} in aqueous medium and the low efficiency of oxidant agent production at the neutral operation pH (Yu et al. 2015); so in this case, the heterogeneous Fenton reaction plays a dominant role because the ·OH reaction proceeds in the surface of the catalyst.

Raman spectroscopy is a widely used method to study the structure of carbon-based materials. Figure 4a shows the Raman spectra of the MWCNTs, fresh Fe₃O₄/MWCNTs,

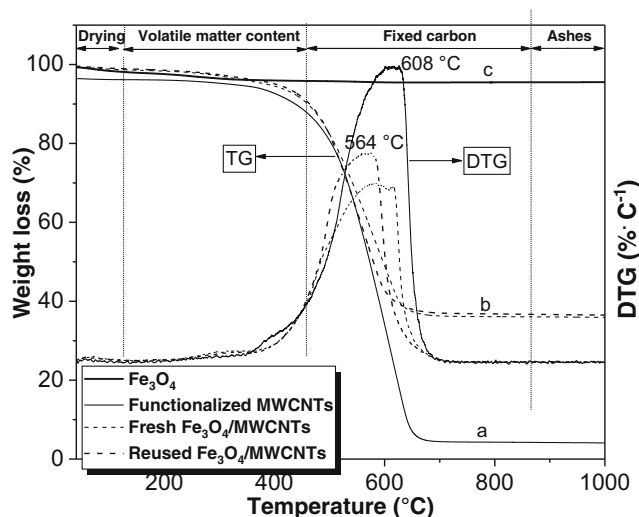**Fig. 2** TGA and DTG analysis of MWCNTs, Fe_3O_4 and Fe_3O_4/MWCNTs

Table 3 Elemental analysis and total iron content of the samples

Samples	Total Fe content	Elemental analysis			
		% C	% H	% N	% S
Functionalized support	n.d.	84.47	0.77	0.19	0.06
Fresh Fe_3O_4/MWCNTs	21.36[a]	57.99	0.85	0.17	0.12
Fe_3O_4/MWCNTs-1	22.77[a]	54.07	0.96	0.18	0.09
Fe_3O_4/MWCNTs-2	15.18[a]	54.27	0.85	0.16	0.06
Effluent after second cycle	0.1[b]	n.d.	n.d.	n.d.	n.d.
Effluent after third cycle	0.1[b]	n.d.	n.d.	n.d.	n.d.

Solution pH of 6.7

n.d. not detected

[a] Milligrams found in 130 mg of catalyst

[b] Milligrams per liter, 3 h reaction time

and the reused catalyst after the second cycle. It could be confirmed that the support and the catalyst showed some differences in their crystallinity. Thus, both materials showed two overlapping peaks in the first-order Raman spectra (disorder-induced (D_1) and graphitic (G_1) peaks, at 1360 and

1600 cm^{-1}, respectively, characteristic of amorphous materials, and exhibited the S band (2700 cm^{-1}), more intense in the spectrum of the support, related to the crystallographic ordering of the structure (Thomberg et al. 2011). The I_G/I_D ratio was evaluated for MWCNTs and Fe_3O_4/MWCNTs, finding that the value slightly increased from 1.34 to 1.44 after
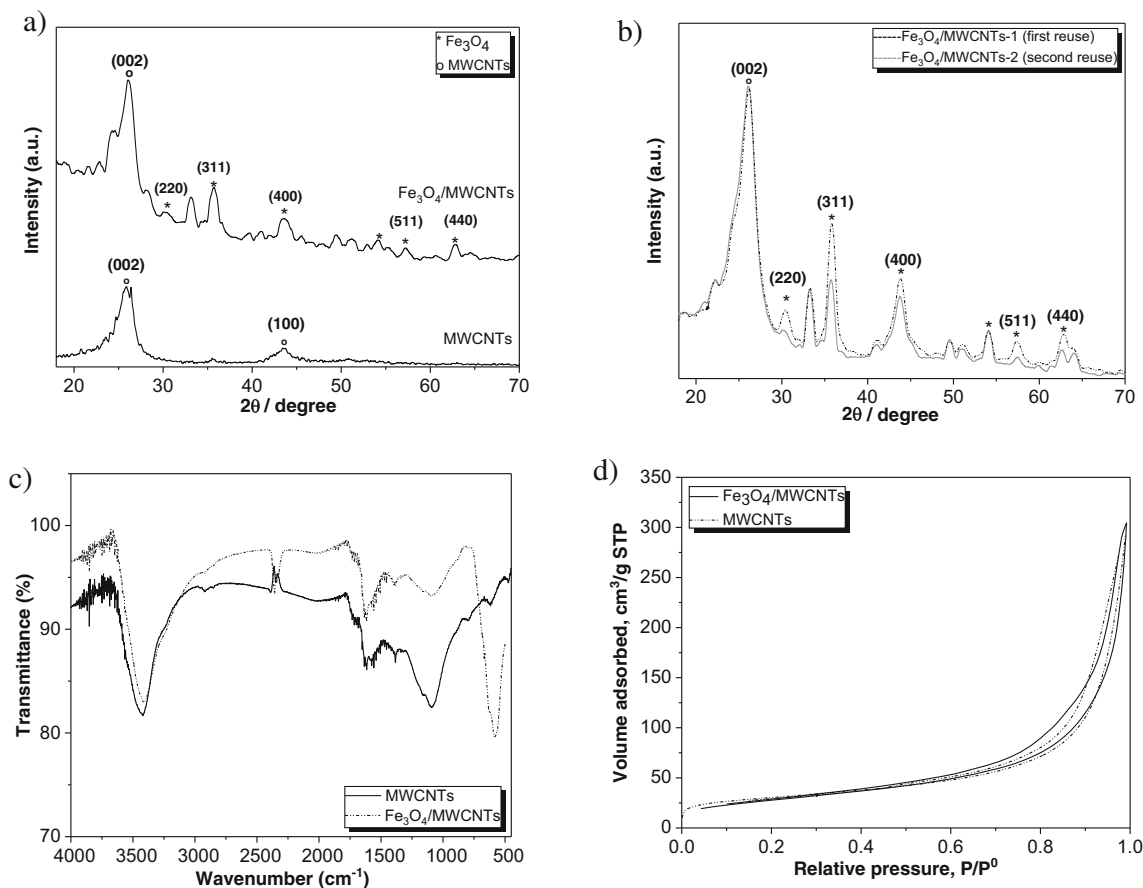

Fig. 3 a) XRD patterns of support and Fe_3O_4/MWCNTs catalyst, b) XRD patterns of Fe_3O_4/MWCNTs-1 and Fe_3O_4/MWCNTs-2 catalysts; c) FT-IR spectra of MWCNTs and Fe_3O_4/MWCNTs; d) N_2 adsorption-desorption isotherms at 77 K of the support and Fe_3O_4/MWCNTs catalyst

Fig. 4 a) Raman spectra of MWCNTs, Fe_3O_4/MWCNTs and Fe_3O_4/MWCNTs-2; b) Magnetization curves of fresh Fe_3O_4/MWCNTs and Fe_3O_4/MWCNTs-2
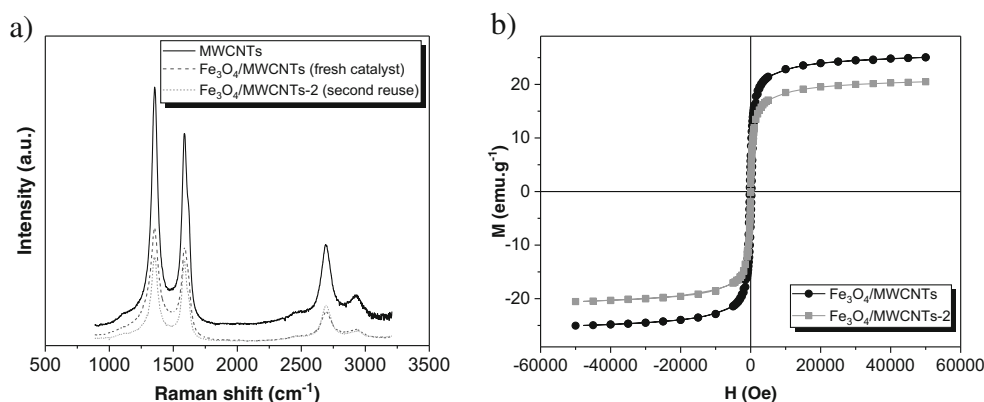
Fe_3O_4 loading in the catalyst. The increase of this ratio suggested that the atomic ordering of the MWCNTs was enhanced after the incorporation of the active phase and the structural defects were modified. The peak centered at 2682.4 cm^{-1} could be assigned to D* band characteristic of MWCNTs (Zhang et al. 2018).

One of the interesting features of using Fe_3O_4/MWCNT catalysts in CWPO reactions is the advantage of being able to easily recover them from the reaction medium after use, due to their magnetic properties. In this sense, the magnetization curves of the fresh Fe_3O_4/MWCNTs and second reused catalysts were investigated to check their superparamagnetic properties (Fig. 4b). In the figure, hysteresis loop in the magnetization curves of both materials could not be observed, while the magnetic remanence and coercive force were 0, illustrating that Fe_3O_4/MWCNT materials can be considered as superparamagnetic. The saturation magnetization (M_s) values of the fresh and second reused catalysts were 20.0 and 25.0 emu g^{-1} at 300 K. According to the results reported by Fan and Li (2012), a saturation magnetization value of 16.3 emu g^{-1} is enough to allow the magnetic separation of the catalyst from the solution with a magnet. These results showed that the fresh and the reused catalysts can be manipulated by an external magnetic field, thus providing a potential advantage for the separation, recovery, and reuse of the catalysts.

Box-Behnken design for the optimization of DCF removal

The CWPO performance of the removal of DCF was evaluated with the variation of different operating variables (Alimohammadi et al. 2017; Rumky et al. 2018). The removal efficiency of DCF (η_N) determined at the steady state can be defined by Eq. 6 and it was calculated at several operation conditions (Table 2). The system variables include three-level incomplete factorial designs (see Table S1).

$$\eta_N = \frac{(C_{N0} - C_N)}{C_{N0}} \qquad (6)$$

A quadratic polynomial response surface model was found to represent the relationship between DCF removal percentage and the independent input variables. Equation 7, obtained by the BBD model, can be used to fit the experimental data.

$$Y = 319.804 - 19.675A - 133.455B - 9.268C + 7.339A^2$$
$$+ 116.073B^2 + 0.097C^2 \qquad (7)$$

where A, B, C, and Y are the initial H_2O_2 dosage (mM), catalyst dosage (g L^{-1}), temperature (°C), and DCF removal efficiency (%), respectively.

The obtained equation demonstrated the accuracy of the experiments and only 3.35% of the total variation cannot be explained, which ensures the goodness of the fit ($R^2 = 0.9665$) (Alexander et al. 2015). F (38.51) and p (0.0000178) values were obtained with a pure error of 0.28 and the predicted error variance (3.00) indicated the validity of the model (see Table 4) (Abdullah et al. 2012; Santiago et al. 2018). The strong linear correlation between the experimental and the predicted values of DCF removal efficiency (Fig. S2) demonstrated that the proposed model is accurate for investigating the effect of the three operation parameters.

All the terms of the model and significance of each term in the obtained regression model are listed in Table 5. The p-values of the quadratic interactions (AB, AC, and BC), not shown in Table 5, are not significant because of $p = 0.05$; all the other terms are significant. That means the predicted model mostly explains the probability of occurrence.

Table 4 Analysis of variance (ANOVA) of the quadratic polynomial model

	df	SS	MS	F	Prob > F (p value)
Regression	6	2083.42	347.24	38.51	0.0000178
Residual	8	72.13	9.01		
Total	14	2155.56			

$R^2 = 0.966$, adj. $R^2 = 0.941$, $S = 2.27$

df degrees of freedom, S mean deviation

Table 5 P test significance of model terms in the quadratic polynomial model

Model	Model coefficient	Estimated coefficient	Standard error	T stat	P value	Degree of significance
Intercept	β_0	319.80	46.42	6.89	0.000	Significant
A	β_1	-19.67	9.18	-2.14	0.065	Possibly significant
B	β_2	-133.45	40.66	-3.28	0.011	Significant
C	β_3	-9.27	1.65	-5.60	0.001	Significant
A^2	B_{11}	7.34	2.49	2.94	0.019	Significant
B^2	β_{22}	116.07	26.17	4.43	0.002	Significant
C^2	B_{33}	0.09	0.02	5.94	0.000	Significant

The uncertainty of the model has been reduced by using the BBD model. The coefficients of the model are an important aspect to take account the uncertainty of the model, in which insignificant model coefficients are present.

In this particular situation, the majority of individual coefficients have p values that are significant except the quadratic interactions (AB, AC, CB). Since the effect of AB, AC, and BC on the operating parameters is representative on the overall effect of the obtained model, these terms are negligible in the model prediction (Table 4) (Salari et al. 2018; Xu et al. 2013). Thus, the model can be represented by Eq. 7.

The reported model showed an optimum DCF removal efficiency of 96.9%, whereas the experimental DCF removal percentage was 95.0% (optimum value in Table 6). Hence, the predictions of the regression model using the RSM showed an average value of deviation of 2.27% with the experimental results. Due to the very small value of deviation, it could be concluded that the prediction of the developed model showed a high accuracy.

The response surface and corresponding contour plots allow to establish the quantitative analysis of the main interaction effects of experimental variables and their contribution in predicting the response. Figure 5 depicted 3D response surface plots, showing the relationship of catalyst and H_2O_2 doses (Fig. 5a), catalyst dose and temperature (Fig. 5b), and H_2O_2 dosage and temperature (Fig. 5c) on the pollutant removal and Fig. 5d shows a contour plot of the effect of the catalyst dose and temperature on DCF removal. The performance of the process was optimized by BBD model considering the minimization of the operating costs on maximum DCF removal. The obtained optimum operating parameters were 1.0 g L^{-1} of catalyst, 2.7 mM of H_2O_2, and 60 °C in 3 h reaction time. It is noteworthy to mention that the model can provide predicted solutions when targeting specific response values, despite the significant effects of interaction between the independent variables were not observed. As it has been reported in the literature, generally, an increase in the catalyst load will lead to the improvement of the $^\bullet$OH radical formation and the subsequent enhancement of the pollutant degradation, because of a greater number of active sites available in the catalyst (Pliego et al. 2015). The results observed in Fig. 5. are in agreement to this statement.

The effect of the H_2O_2 concentration on CWPO process was similar to that found for the catalyst load. Within a determined range surrounding the stoichiometric value of H_2O_2, an increase in the dosage of H_2O_2 enhanced the oxidative degradation of DCF due to the promotion of $^\bullet$OH formation in the CWPO process (Moffett & Kiza 1987; Ma et al. 2015; Ribeiro et al. 2016a). Nevertheless, at the used working pH, the increase of H_2O_2 concentration had a slight effect on the decrease in the pollutant removal. At close to neutral pH, the H_2O_2 dose did not have a crucial effect on the DCF removal, comparing to conditions usually found in Fenton reactions (pH = 3), when a high temperature (60 °C) was used and an iron-based material was acting as a catalyst (Munoz et al. 2017; Nair and Kurian 2017). Thus, temperature values of 60 °C or below did not seem to have a great influence on the decomposition of H_2O_2 in H_2O and O_2.

Model evaluation

The evolution of the DCF removal and the consumption of H_2O_2 along the reaction time at the different tested operating parameters defined in the variable coded levels (Table S1) can be observed in Figs. S3 and S4, respectively. Regarding the effect of the temperature, it could be observed that the increase of up to 60 °C had a positive effect on the CWPO reaction, enhancing both DCF removal and consumption efficiency of H_2O_2. As it could be observed in Fig. S3, the increase in the load of catalyst enhanced the removal of DCF, as H_2O_2 concentration did.

The experiments allowed to determine the optimal experimental conditions for DCF removal by CWPO reaction, $T = 60$ °C, $pH_0 = 6.7$, $[H_2O_2]_0 = 2.7$ mM, and [catalyst] = 1.0 g·L^{-1}, obtaining 95%, 90%, and 75% of DCF degradation values in 180, 120, and 10 min reaction time, respectively, measuring a pH value of 6.7 in the reaction effluent.

From the results, it could be concluded that the synthesized Fe_3O_4/MWCNT material is a highly active and robust catalyst

Table 6 DCF removal percentage—observed and predicted—at the optimum operation conditions

Actual values			DCF removal efficiency (%)	
A: $[H_2O_2]_0$ (mM)	B: [catalyst] (g L^{-1})	C: temperature (°C)	Observed	Predicted
2.7	1.0	60	95.0	96.9

in comparison to another iron-based systems using similar DCF initial concentrations (see Table 1).

Reaction kinetics and activation energy for CWPO of DCF

The CWPO experiments of DCF were performed at different temperatures (40, 50, and 60 °C), maintaining constant values of initial H_2O_2 dosage (2.7 mM), initial pH (6.7), and initial catalyst dose (1.0 g L^{-1}). All the experiments were accomplished during 3 h reaction time.

Firstly, the initial reaction rate (k_0, mmol min^{-1} g_{cat}^{-1}) values were calculated at the tested temperatures, resulting in 2.94, 3.49, and 4.33 · 10^{-3} mmol min^{-1} g_{cat}^{-1} for 40, 50, and 60 °C, respectively (Table 7). As it can be observed, the temperature showed a high influence on the oxidative process, observing a difference of one and two magnitude orders in the initial reaction rate values, for the tested temperatures.

Secondly, the kinetic evolution of DCF removal by using Fe_3O_4/MWCNT catalyst by CWPO was also discussed at the different tested temperatures. The initial fast removal process mainly results from the high concentration of $^\bullet$OH radicals and DCF in the aqueous medium. Generally, at these conditions, the degradation of DCF by CWPO process should be described as a pseudo-second-order reaction. In this context, the obtained data from DCF removal at the three different tested temperatures were fitted to a pseudo-second-order model in order to describe the kinetic evolution of DCF. This model was proposed by Haji et al. (Haji et al. 2015) for the heterogeneous degradation of azo dyes by CWPO reaction. The pseudo-second-order model can be described by Eq. 7 and represented by its integrated form at a constant-density batch reactor (Eq. 8):

$$-r = k\left(C - C^*\right)^2 \qquad (7)$$

$$C = C^* + \cfrac{1}{\cfrac{1}{C_0 - C^*} + kt} \qquad (8)$$

where k (L mg^{-1} h^{-1}) is the pseudo-second-order rate constant
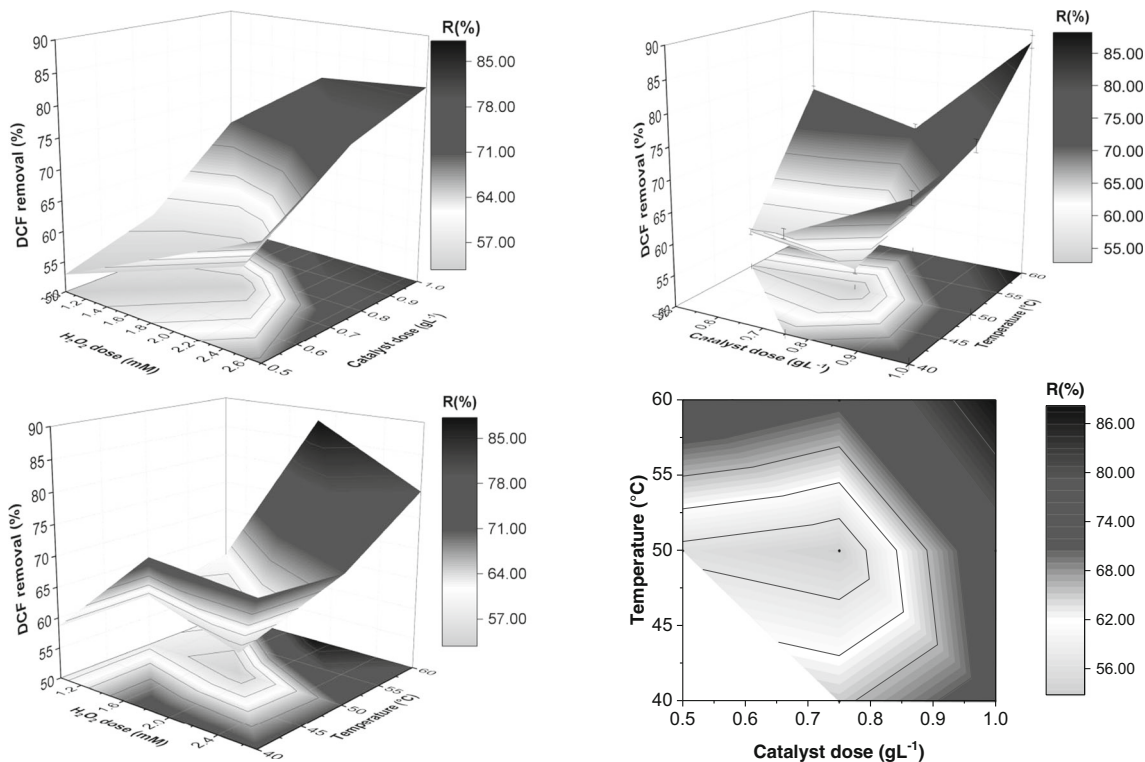

Fig. 5 Combined effect of (a) H_2O_2 dose vs. catalyst; (b) catalyst dosage vs. temperature; (c) H_2O_2 dose vs. temperature; (d) Contour plot of temperature and catalyst dose on DCF removal

Table 7 Initial reaction rate values for CWPO of DCF at different temperatures

Temperature (°C)	40	50	60
k_0 (mmol min^{-1} g$_{cat}^{-1}$) $\times 10^3$	2.94	3.49	4.33
R^2	0.961	0.964	0.964

Reaction conditions: $[DCF]_0 = 10.0$ mg L^{-1}, pH $= 6.7$, [catalyst] $= 1.0$ g L^{-1}, $[H_2O_2]_0 = 2.7$ mM, 3 h reaction time

and C^* (mg L^{-1}) is the minimum concentration of the pollutant in the aqueous solution. Since the resulting equation cannot be linearized, a nonlinear regression analysis was used to estimate k and C^* values (Table 8); thus, the experimental and predicted data are depicted in Fig. 6. As it can be seen, the pseudo-second-order model successfully described the experimental data. So, the estimated apparent rate constants increased with the temperature, e.g., 0.227, 0.528, and 1.150 L mg^{-1} h^{-1}, for 40, 50, and 60 °C, respectively. The first value was similar to that reported by Haji et al. (2015) in the treatment of an azo dye at room temperature.

The activation energy (E_a) value for DCF removal was calculated by Arrhenius equation (Fig. 7), obtaining a value of 70.30 kJ mol^{-1}. The found value was much higher than those reported for diffusion-controlled reactions, which usually ranged from 10 to 13 kJ mol^{-1} (Lin and Gurol 1998; Chen et al. 2017). This allowed to assume that in this case the rate in the CWPO reaction was dominated by the intrinsic chemical reaction on the Fe$_3$O$_4$/MWCNT surface rather than the existence of internal/external mass transfer limitations. The internal and external mass transfer diffusion can be discarded due to the small particle size of the catalyst used in the experiments (lower than 100 μm) and the stirring velocity was maintained constant. The obtained activation energy value was close to other values reported in the literature where different heterogeneous catalysts were used for the CWPO degradation of different organic compounds (Xu and Wang 2012; Yan et al. 2016; Nair and Kurian 2017). Thus, the proposed pseudo-second-order kinetic model showed a high accuracy ($R^2 = 0.95$) for the prediction of the experimental data at the tested operating conditions and it showed validity within the highest limits of temperature (60 °C) and H$_2$O$_2$ concentration (2.7 mM).

Table 8 Apparent rate constant values for CWPO of DCF at different temperatures

T (°C)	Pseudo-second-order model[a]		
	C^* (mg L^{-1})	k (L mg^{-1} h^{-1})	R^2
40	0.83	0.227	0.991
50	1.36	0.528	0.995
60	0.59	1.150	0.997

[a] Reaction conditions: $[DCF]_0 = 10.0$ mg L^{-1}, pH $= 6.7$, [catalyst] $= 1.0$ g L^{-1}, $[H_2O_2]_0 = 2.7$ mM, 3 h reaction time
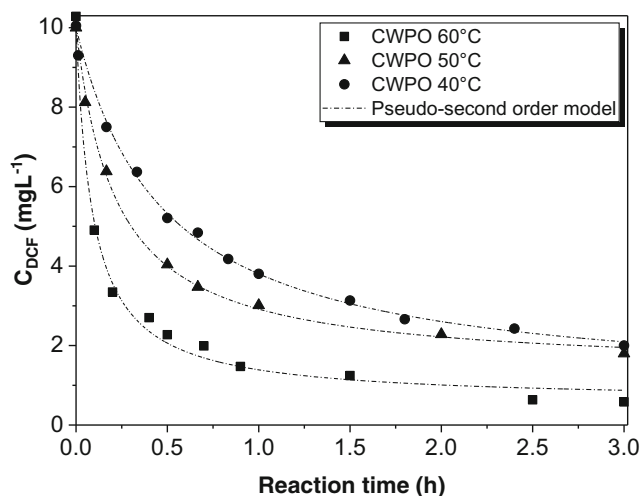

Fig. 6 DCF removal evolution by CWPO predicted by pseudo-second-order model at three different tested temperatures ($[H_2O_2]_0 = 2.7$ mM, $[DCF]_0 = 10.0$ mg·L^{-1}, pH$_0 = 6.7$, [catalyst] $= 1.0$ g·L^{-1})

Stability and reusability of the catalyst

One of the most important challenges of CWPO reactions is related to the deactivation of the catalyst. Thus, the evaluation of the stability of the catalyst was assessed using the solid in three consecutive cycles after drying the solid overnight at 60 °C. In this case, the reusability tests were accomplished at the optimum operation conditions ($T = 60$ °C, $[H_2O_2]_0 = 2.7$ mM, [catalyst] $= 1.0$ g·L^{-1}, pH$_0 = 6.7$; see Table 6). The three consecutive runs of DCF degradation are depicted in Fig. 8, where an outstanding stability of the catalyst could be observed, since the DCF removal efficiency (95%) remained constant in 3 h reaction time along the subsequent experiments.

Nevertheless, the results obtained in this work are significantly better than those obtained by Singh and Lo
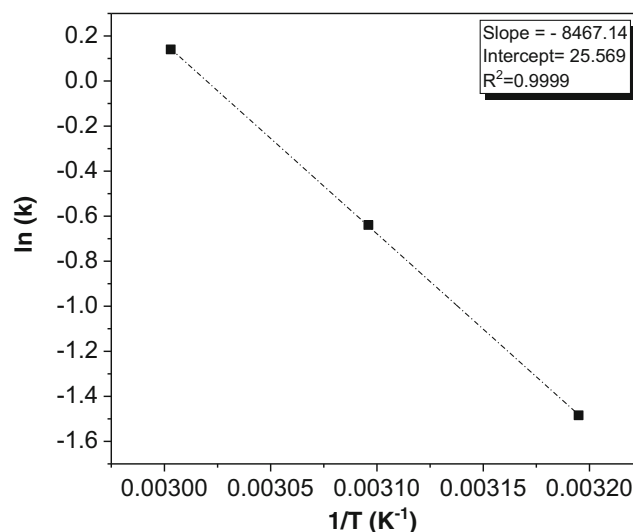

Fig. 7 Arrhenius plot for CWPO of DCF ($[H_2O_2]_0 = 2.7$ mM, $[DCF]_0 = 10.0$ mg·L^{-1}, pH$_0 = 6.7$, [catalyst] $= 1.0$ g·L^{-1})
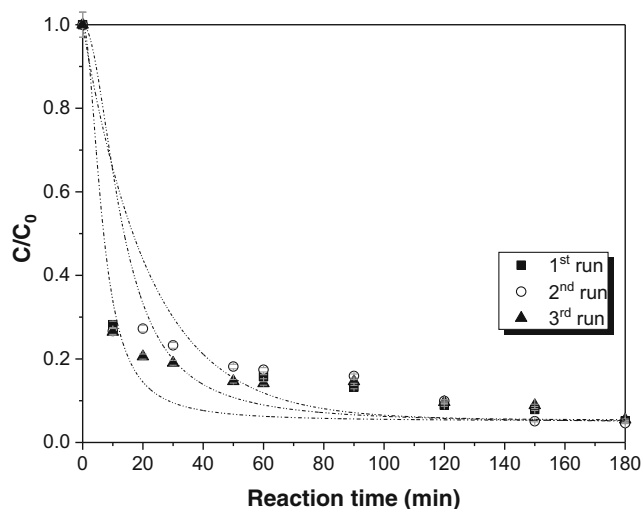
Fig. 8 Performance of the catalyst upon three sequential CWPO runs of DCF (T = 60 °C, $[DCF]_0 = 10$ mg·L^{-1}, $[H_2O_2]_0 = 2.7$ mM, [catalyst] = 1.0 g·L^{-1}, $pH_0 = 6.7$)

(Singh and Lo 2017) in the CWPO degradation of pyridine with metal oxides as catalysts, who observed that the removal of the drug decreased from 95% in the first run to 82% in the third cycle of reaction.

Iron leaching and blank tests

These experiments were conducted at 70 °C and pH of 6.7 only with the catalyst support in the absence of oxidant (adsorption MWCNT test), with the catalyst in absence of oxidant (adsorption Fe$_3$O$_4$/MWCNT test), only with hydrogen peroxide (2.7 mM) in the absence of a catalyst (H$_2$O$_2$ test) and with hydrogen peroxide (2.7 mM) and 10.0 mg L^{-1} of dissolved Fe^{+3} ions (homogeneous reaction test). The homogeneous reaction was carried out in order to measure the DCF removal value and compare it with the DCF removal obtained by heterogeneous reaction at pH 6.7. The DCF removal profiles of all the blank experiments and the heterogeneous catalytic run (Fe$_3$O$_4$/MWCNTs + H$_2$O$_2$) as well can be found in Fig. S5 (Supplementary Material).

Same values of DCF removal (12%) were found by using only both the support and catalyst in the absence of hydrogen peroxide, after 3 h reaction time, due to the adsorption of the pollutant onto the surface of the solid, which indicates that DCF is mainly removed via oxidation. The potential of hydrogen peroxide in the absence of the catalyst (H$_2$O$_2$ test) was almost negligible, confirming the effective degradation of DCF by CWPO reaction.
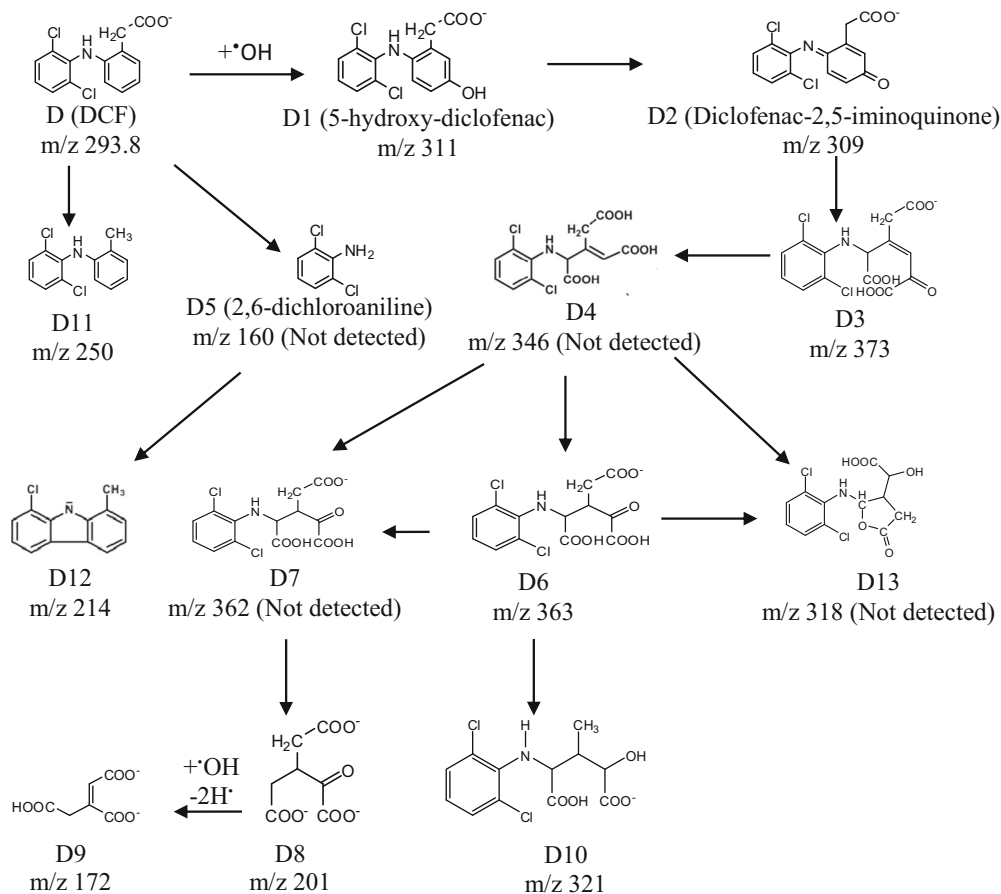

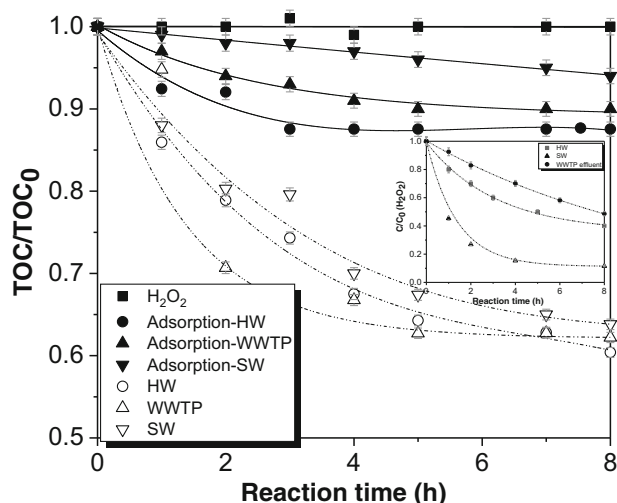**Fig. 9** Proposed degradation pathways of the DCF reaction by CWPO (T = 60 °C, pH $_0$ = 6.7, [catalyst] = 1.0 g·L^{-1}, [H$_2$O$_2$] = 0.5 mM)

Fig. 10 TOC degradation evolution in the three tested real aqueous matrices ($[H_2O_2]_0 = 2.7$ mM, [catalyst] $=1.0$ g·L^{-1}, T $= 60$ °C, non-modified pH). The inserted graph is referred to the decomposition of H_2O_2 with the reaction time

With the homogeneous Fenton test ($[Fe^{+2}] = 10$ mg L^{-1}), a DCF removal below 27% after 3 h reaction time was found (Martínez et al. 2018). Finally, the catalytic activity of Fe_3O_4/MWCNTs in the presence of hydrogen peroxide showed to be notoriously high (95%), indicating that the efficient pollutant removal is due to the synergetic interaction between the catalyst and the $^{•}OH$ radicals in the aqueous medium.

The total dissolved iron concentration of the effluent of the fresh Fe_3O_4/MWCNTs and the reused after three cycle catalysts was analyzed. In both cases, the amount of iron was only 0.1 mg L^{-1} (the total leached Fe was below of the limits assigned by the EU directive, < 2 mg L^{-1}). Therefore, it can be concluded that the leaching of the active phase during the CWPO reaction is negligible, supporting the high stability of the synthesized catalyst.

Degradation products

Intermediates in the CWPO reaction of DCF using Fe_3O_4/MWCNTs after 3 h reaction time, using 0.5 mM of H_2O_2 and 1.0 g L^{-1} of catalyst, were evaluated. A total of 29 peaks (Fig. S6 of Supplementary Material) were detected in the treated DCF sample and 7 peaks in the DCF standard (DCF M = $C_{14}C_{12}H_{10}O_2$; molecular weight = 293.8 gmol^{-1}; t_R =

Table 9 Toxicity values of the tested real aqueous matrices

	WWTP	SW	HW
Initial at 5/15 min (TU)	3.67/3.64	2.53/1.95	5.98/4.28
Final at 5/15 min (TU)	1.30/1.28	1.58/1.51	2.84/2.98
Blank H_2O_2 at 5/15 min (TU)	0.48/0.62	0.35/0.65	2.56/2.08

21.7 min) (Fig. S7). The proposed structures of the intermediates are shown in Table S3. Compared to other advanced oxidation technologies (Hofmann et al. 2007), the amount of obtained intermediate compounds is considerably lower. Based on the structures listed in Table S3, a reaction pathway for the DCF removal by CWPO has been proposed (Fig. 9). The pathway A, 5-hydroxy-diclofenac (D1), indicated a hydroxylation as one of the first reaction steps. Then, diclofenac-2,5-iminoquinone (*m/z* 309) (D2) is formed from D1 (*m/z* 311) by $^{•}OH$ attack and abstraction of H$^{•}$. Subsequent $^{•}OH$ attacks on D2 produce D3 (*m/z* 373) (a molecule containing the aromatic ring cleavage) and then D3 is decarboxylated by $^{•}OH$ attack producing D4 (*m/z* 346). The D4 followed three different pathways producing D5 (*m/z* 318), D6 (*m/z* 363) (detected), and D7 (*m/z* 362) compounds. Next, D7 is attacked by $^{•}OH$ in the NH-bridge. In this reaction, 2-*oxo*-3-(1-carboxymethyl) pentanodioic acid (*m/z* 201) (D8) is formed primarily and possibly 2,6-dichloroaniline (not detected). D8 suffered decarboxylation producing 3-carboxy-pent-2-enedicarboxylic acid (*m/z* 172) (D9). However, D6 produced D10 (*m/z* 321) after its decarboxylation. On the other hand, the degradation pathway B started with the decarboxylation of DCF by the attack of $^{•}OH$ in the aromatic ring and D11 (*m/z* 250) was formed. The chlorine in D11 was substituted by $^{•}OH$ in the ring and then it was removed in the form of water to generate D12 (*m/z* 214) which contains a cycle pentane group between the two aromatic rings. Another pathway C is presented where 2,6-dichloroaniline is formed primarily.

Proof of concept: application of CWPO to environmentally relevant water matrices

Most of the studies in the literature have been commonly accomplished using deionized water, an interesting fact for the initial design of the experiments as well as comparison purposes. So, the proposed process must be effective in complex water matrices that contain multiple natural and anthropogenic compounds (Rizzo et al. 2013). As a proof of concept, the performance of the CWPO reaction was evaluated using different real water matrices, such as a WWTP effluent, a surface water (SW), and a hospital wastewater (HW).

The main macroscopic characterization of the real wastewater is collected in Table S4 (Supplementary Material). Briefly, the TOC concentrations of the hospital water, surface water, and WWTP effluent were 110, 6.8, and 9.8 mg L^{-1}, respectively. With regard to the suspended solids, the hospital and surface wastewater showed the highest concentrations (138 and 140 mg L^{-1}, respectively). Figure 10. shows the results obtained in the CWPO of the abovementioned water matrices. The three tested real matrices were efficiently treated by CWPO with the synthesized catalyst, achieving a TOC removal efficiency for all the matrices of 60% after 8 h reaction time. Thus, the presence of a high content of organic

compounds in the hospital wastewater led to detrimental effects on the kinetic rate of the process, observing an inhibition effect in the initial stage of the reaction. From our knowledge, the organic species present in the wastewater compete for the active sites of the catalyst by adsorption, hindering the removal efficiency (Ribeiro et al. 2016b). The same inhibition stage was observed in the degradation experiment of the surface water, possibly attributed to the large amount of solids present in the matrix.

The ecotoxicity of the treated effluents is an interesting parameter to determine the effectiveness of a wastewater treatment technology. The ecological risk associated to a real wastewater is usually underestimated, if the toxicological information obtained through bioassays is not bear in mind. It has been widely reported that the pharmaceutical compounds such as DCF are released into the environmental effluents. In this context, Álvarez-Torrellas et al. (Álvarez-Torrellas et al. 2017) and Rimayi et al. (Rimayi et al. 2018) have been already recorded the presence of these drugs in real effluents, describing them as common contaminants in surface water, hospital, and WWTP effluents.

In this work, the evaluation of the ecotoxicity of the untreated and treated real wastewater effluents by CWPO was assessed using the *V. fischeri* test. This test, based on the natural emission of the luminescent bacteria *V. fischeri*, has been selected because it is cost-effective, reproducible, and does not suppose ethical problems ensuing from the use of higher organisms such as fish and rat (De García et al. 2014). Ecotoxicity tests were carried out by duplicate with a control solution and the data were statistically processed by the Microtox® software, as well as the results were expressed as TUs after 5 and 15 min of exposure.

As it has been expected, the highest ecotoxicity values (TU = 5.98 and 4.28, after 5 and 15 min of exposure, respectively) was obtained for the hospital wastewater, since the surface water and WWTP effluent showed lower TU values (2.53, 1.95, 3.67, and 3.64, respectively). Thus, as it can be observed in Table 9, the CWPO treatment led to a remarkable decrease in the ecotoxicity of the real aqueous matrices.

Despite the decrease in the toxicity of the three real matrices, the hospital and WWTP effluents remained slightly toxic even after the CWPO treatment. This behavior has been related in the literature with the presence of trace amounts of H_2O_2 or the formation of toxic by-products along the reaction (De Vera et al. 2015; Esteban García et al. 2018). This could be assessed by the measurement of the toxicity assigned to the quantities of H_2O_2 that remained in the effluent after the CWPO reaction, which must take into account the three cases.

In terms of toxicity, the United States Environmental Protection Agency (US EPA) (2004) and the European Chemicals Agency (ECHA) (2018) have established the following classification: $0 < TU \leq 0.07$ for low toxicity, $0.07 < TU \leq 2.67$ for medium toxicity, $2.67 < TU \leq 5.86$ for high

toxicity, and $TU > 5.86$ for very high toxicity. With this criterion, the toxicity of the three real aqueous matrices after the CWPO treatment could be classified as medium toxicity.

Consequently, based on the achieved results, the CWPO using Fe_3O_4/MWCNTs as a catalyst represents a clearly advantageous and environmentally friendly technology for ensuring a partial/total elimination of the ecotoxicity of real aqueous matrices.

Conclusions

In this study, Fe_3O_4/MWCNT catalyst was successfully prepared and used as a highly active material for DCF removal in catalytic wet peroxide oxidation. Due to the dispersion of Fe_3O_4 nanoparticles on MWCNTs (studied by transmission electron microscopy), a synergistic effect between the iron-based catalyst and the $^{\bullet}OH$ radicals generated in the reaction medium was achieved. Consequently, this material exhibited a high catalytic activity for DCF removal. Investigations on the effect of operation parameters (temperature, H_2O_2 concentration, and catalyst load) by the response surface methodology were accomplished. Under the optimal conditions ($T = 60$ °C, $[H_2O_2]_0 = 2.7$ mM, [catalyst] = 1.0 g L^{-1}), the DCF degradation and H_2O_2 mineralization were 95% (maintained constant after three consecutive cycles) and 85%, respectively, observing an outstanding stability and reusability of the as-prepared catalyst. Finally, the versatility of the catalyst was demonstrated in the treatment of environmentally relevant aqueous matrices, obtaining an effective reduction in the ecotoxicity values. Thus, the catalyst could be easily separated after reaction by an external magnetic field due to the superparamagnetic properties of the particles.

References

Abdullah AH, Melanie-Moey HJ, Yusol NA (2012) Response surface methodology analysis of the photocatalytic removal of Methylene Blue using bismuth vanadate prepared via polyol route. J Environ Manag 24:1694–1701

Alexander DLJ, Tropsha A, Winkler DA (2015) Beware of R(2): simple, unambiguous assessment of the prediction accuracy of QSAR and QSPR models. J Chem Inf Model 55:1316–1322

Alimohammadi V, Sedighi M, Jabbari E (2017) Optimization of sulfate removal from wastewater using magnetic multi-walled carbon

nanotubes by response surface methodology. Water Sci Technol 76: 2593–2602

Álvarez-Torrellas S, Peres JA, Gil MV, Ovejero G, García J (2017) Effective adsorption of non-biodegradable pharmaceuticals from hospital wastewater with different carbon materials. Chem Eng J 320:319–329

Álvarez-Torrellas S, Munoz M, Gläsel J, de Pedro ZM, Domínguez CM, García J, Etzold BJM, Casas JA (2018) Highly efficient removal of pharmaceuticals from water by well-defined carbide-derived carbons. Chem Eng J 347:595–606

Ashfaq M, Khan KN, Rehman MSU, Mustafa G, Nazar MF, Sun Q, Iqbal J, Mulla SI, Yu C-P (2017) Ecological risk assessment of pharmaceuticals in the receiving environment of pharmaceutical wastewater in Pakistan. Ecotox Environ Safe 136:31–39

Ayazi Z, Khoshhesab ZM, Norouzi S (2016) Modeling and optimizing of adsorption removal of Reactive Blue 19 on the magnetite/graphene oxide nanocomposite via response surface methodology. Desalin Water Treat 57:25301–25316

Benítez FJ, García J, Acero JL, Real FJ, Roldan G (2011) Non-catalytic and catalytic wet air oxidation of pharmaceuticals in ultra-pure and natural waters. Process Saf Environ Prot 89:334–341

Buzarovska A, Stefov V, Najdoski M, Bogoeva-Gaceva G (2015) Thermal analysis of multi-walled carbon nanotubes material obtained by catalytic pyrolysis of polyethylene. Maced J Chem Chem Eng 34:373–379

Chen D, Chen S, Jiang Y, Xie S, Quang H, Hua L, Luo X, Guo L (2017) Heterogeneous Fenton-like catalysis of Fe-MOF derived magnetic carbon nanocomposites for degradation of 4-nitrophenol. RSC Adv 7:49024–49030

Chen F, Yang Q, Wang DB, Yao FB, Ma YH, Li XM, Wang JJ, Jiang LH, Wang LL, Yu HQ (2018) Highly-efficient degradation of amiloride by sulfate radicals-based photocatalytic processes: reactive kinetics, degradation products and mechanism. Chem Eng J 354:983–994

Chong S, Zhang G, Zhang N, Liu Y, Huang T, Chang H (2017) Diclofenac degradation in water by FeCeOx catalyzed H_2O_2: influencing factors, mechanism and pathways. J Hazard Mater 334:150–159

Das R, Abd Hamid SB, Ali ME, Ismail AF, Annuar MSM, Ramakrishna S (2014) Multifunctional carbon nanotubes in water treatment: the present, past and future. Desalination 354:160–179

De García SAO, Pinto GP, García-Encina PA, Irusta-Mata R (2014) Ecotoxicity and environmental risk assessment of pharmaceuticals and personal care products in aquatic environments and wastewater treatment plants. Ecotoxicol 23:1517–1533

De Vera GA, Stalter D, Gemjak W, Weinberg HS, Keller J, Farré MJ (2015) Towards reducing DBP formation potential of drinking water by favouring direct ozone over hydroxyl radical reactions during ozonation. Water Res 87:49–58

Deng Y, Zhao R (2015) Advanced oxidation processes (AOPs) in wastewater treatment. Curr Pollut Reports 1:167–176

Do QC, Kim D-G, Ko S-O (2018) Catalytic activity enhancement of a Fe_3O_4@SiO_2 yolk-shell structure for oxidative degradation of acetaminophen by decoration with copper. J Clean Prod 172:1243–1253

Ebele AJ, Abdallah MAE, Harrad S (2017) Pharmaceuticals and personal care products (PPCPs) in the freshwater aquatic environment. Emerg Contam 3:1–16

Esteban García B, Rivas G, Arzate S, Sánchez Pérez JA (2018) Wild bacteria inactivation in WWTP secondary effluents by solar photo-Fenton at neutral pH in raceway pond reactors. Catal Today 313:72–78

European Chemicals Agency (ECHA) (2018) Commission staff working document accompanying the document Communication from the Commission of the European Economic and Social Committee. Commission General Report on the operation of REACH and review of certain elements Conclusions and Actions. SWD/2018/058 final

Fan X-J, Li X (2012) Preparation and magnetic property of multiwalled carbon nanotubes decorated by Fe_3O_4 nanoparticles. New Carbon Mater 27:1–5

Ferreira SLC, Bruns RE, Ferreira HS, Matos GD, David JM, Brandão GC, da Silva EGP, Portugal LA, dos Reis PS, Souza AS, dos Santos WNL (2007) Box-Behnken design: an alternative for the optimization of analytical methods. Anal Chim Acta 597:179–186

Fischer A, ter Laak T, Bronders J, Desmet N, Christoffels E, van Wezel A, van der Hoek JP (2017) Decision support for water quality management of contaminants of emerging concern. J Environ Manag 193: 360–372

Gao G, Chu W, Chen Z, Shen J (2017) Catalytic ozonation of diclofenac with iron silicate-loaded pumice in aqueous solution. Water Sci Technol 17:1458–1467

Garcia J, Gomes HT, Serp P, Kalck P, Figueiredo JL, Faria JL (2006) Carbon nanotube supported ruthenium catalysts for the treatment of high strength wastewater with aniline using wet air oxidation. Carbon 44:2384–2391

Haji S, Khalaf M, Shukrallah M, Abdullah J, Ahmed S (2015) A kinetic comparative study of azo dye decolorization by catalytic wet peroxide oxidation using Fe-Y zeolite/H_2O_2 and photooxidation using UV/H_2O_2. React Kinet Mech Catal 114:795–815

Hofmann J, Freier U, Wecks M, Hohmann S (2007) Degradation of diclofenac in water by heterogeneous catalytic oxidation with H_2O_2. Appl Catal B-Environ 70:447–451

Khan AH, Kim J, Sumarah M, Macfie SM, Ray MB (2017) Toxicity reduction and improved biodegradability of benzalkonium chlorides by ozone/hydrogen peroxide advanced oxidation process. Sep Purif Technol 185:72–82

Krstic V, Urosevic T, Pesovski B (2018) A review on adsorbents for treatment of water and wastewaters containing copper ions. Chem Eng Sci 192:273–287

Li X, Wang TC, Qu GZ, Liang DL, Hu SB (2016) Enhanced degradation of azo dye in wastewater by pulsed discharge plasma coupled with MWCNTs-TiO_2/gamma-Al_2O_3 composite photocatalyst. J Environ Manag 172:186–192

Lin S-S, Gurol MD (1998) Catalytic decomposition of hydrogen peroxide on iron oxide: kinetics, mechanism, and implications. Environ Sci Technol 32:1417–1423

Luo Y, Guo W, Ngo HH, Nghiem LD, Hai FI, Zhang J, Liang S, Wang XC (2014) A review on the occurrence of micropollutants in the aquatic environment and their fate and removal during wastewater treatment. Sci Total Environ 473-474:619–641

Ma J, Y M, Yu F, Chen J (2015) Easy solid-phase synthesis of pH-insensitive heterogeneous CNTs/FeS Fenton-like catalyst for the removal of antibiotics from aqueous solution. J Colloid Interf Sci 444:24–32

Martínez F, Leo P, Orcajo G, Díaz-García M, Sanchez-Sanchez M, Calleja G (2018) Sustainable Fe-BTC catalyst for efficient removal of methylene blue by advanced Fenton oxidation. Catal Today 313: 6–11

Moffett JD, Zika RG (1987) Reaction kinetics of hydrogen peroxide with copper and iron in seawater. Environ Sci Technol 21:804–810

Munoz M, Mora FJ, De Pedro ZM, Alvarez-Torrellas S, Casas JA (2017) Application of CWPO to the treatment of pharmaceutical emerging pollutants in different water matrices with a ferromagnetic catalyst. J Hazard Mater 331:45–54

Nair DS, Kurian M (2017) Catalytic peroxide oxidation of persistent chlorinated organics over nickel-zinc ferrite nanocomposites. J Water Process Eng 16:69–80

Oaks JL, Gilbert M, Virani MZ, Watson RT, Meteyer CU, Rideout BA, Shivaprasad HL, Ahmed S, Chaudhry MJ, Arshad M, Mahmood S, Ali A, Khan AA (2004) Diclofenac residues as the cause of vulture population decline in Pakistan. Nature 427:630–633

Ovejero G, Sotelo JL, Romero MD, Rodríguez A, Ocana MA, Rodríguez G, Garcia J (2006) Multi-walled carbon nanotubes for liquid-phase

oxidation. Functionalization, characterization, and catalytic activity. Ind Eng Chem Res 45:2206–2212

Ovejero G, Sotelo JL, Rodriguez A, Diaz C, Sanz R, Garcia J (2007) Platinum catalyst on multi-walled carbon nanotubes for the catalytic wet air oxidation of phenol. Ind Eng Chem Res 46:6449–6455

Pinho MT, Gomes HT, Ribeiro RS, Faria JL, Silva AMT (2015) Carbon nanotubes as catalysts for catalytic wet peroxide oxidation of highly concentrated phenol solutions: towards process intensification. Appl Catal B-Environ 165:706–714

Pliego G, Zazo JA, Garcia-Munoz P, Munoz M, Casas JA, Rodriguez JJ (2015) Trends in the intensification of the Fenton process for waste-water treatment: an overview. Crit Rev Environ Sci Technol 45: 2611–2692

Ribeiro RS, Frontistis Z, Mantzavinos D, Venieri D, Antonopoulou M, Konstantinou I, Silva AMT, Faria JL, Gomes HT (2016a) Magnetic carbon xerogels for the catalytic wet peroxide oxidation of sulfa-methoxazole in environmentally relevant water matrices. Appl Catal B-Environ 199:170–186

Ribeiro RS, Silva AMT, Figueiredo JL, Faria JL, Gomes HT (2016b) Catalytic wet peroxide oxidation: a route towards the application of hybrid magnetic carbon nanocomposites for the degradation of organic pollutants. A review. Appl Catal B-Environ 187:428–460

Ribeiro RS, Rodrigues RO, Silva AMT, Tavares PB, Carvalho AMC, Figueiredo JL, Faria JL, Gomes HT (2017) Hybrid magnetic gra-phitic nanocomposites towards catalytic wet peroxide oxidation of the liquid effluent from a mechanical biological treatment plant for municipal solid waste. Appl Catal B-Environ 219:645–657

Rimayi C, Odusanya D, Weiss JM, de Boer J, Chimuka L (2018) Contaminants of emerging concern in the Hartbeespoort Dam catch-ment and the uMngeni River estuary 2016 pollution incident. South Africa Sci Total Environ 627:1008–1017

Rizzo L, Manaia C, Merlin C, Schwartz T, Dagot C, Ploy MC, Michael I, Fatta-Kassinos D (2013) Urban wastewater treatment plants as hotspots for antibiotic resistant bacteria and genes spread into the environment: a review. Sci Total Environ 447:345–360

Rumky J, Ncibi MC, Burgos-Castilla RC, Deb A, Sillanpää M (2018) Optimization of integrated ultrasonic-Fenton system for metal re-moval and dewatering of anaerobically digested sludge by Box-Behnken design. Sci Total Environ 645:573–584

Salari M, Rakhshandehroo GR, Nikoo MR (2018) Degradation of cipro-floxacin antibiotic by homogeneous Fenton oxidation: hybrid AHP-PROMETHEE method, optimization, biodegradability improve-ment and identification of oxidized by-products. Chemosphere 206:157–167

Santiago DE, González-Díaz O, Arana J, Mellan EP, Pérez-Pena J, Dona-Rodríguez JM (2018) Factorial experimental design of imazalil-containing wastewater to be treated by Fenton-based processes. J Photochem Photobiol A 353:240–250

Sharma RK, Dutta S, Sharma S, Zboril R, Varma RS, Gawande MB (2016) Fe_3O_4 (iron oxide)-supported nanocatalysts: synthesis, char-acterization and applications in coupling reactions. Green Chem 18: 3184–3209

Singh S, Lo S-L (2017) Catalytic performance of hierarchical metal ox-ides for per-oxidative degradation of pyridine in aqueous solution. Chem Eng J 309:753–765

Sklari SD, Plakas KV, Petsi PN, Zaspalis VT, Karabelas AJ (2015) Toward the development of a novel electro-Fenton system for elim-inating toxic organic substances from water. Part 2. Preparation, characterization, and evaluation of iron-impregnated carbon felts as cathodic electrodes. Ind Eng Chem Res 54:2059–2073

Standard Methods for the Examination of Water and Wastewater (2005) 21st ed.; American Public Health Association/American Water Works Association/Water Environment Federation: Washington, DC

Thomberg T, Kurig H, Jänes A, Lust E (2011) Mesoporous carbide-derived carbons prepared from different chromium carbides. Micropor Mesopor Mater 141:88–93

USEPA (2004) NPDES compliance inspection manual, EPA 305-X-03-004

Verlicchi P, Al Aukidy M, Zambello E (2012) Occurrence of pharmaceu-tical compounds in urban wastewater: removal, mass load and en-vironmental risk after a secondary treatment—a review. Sci Total Environ 429:123–155

Wang Q, Jiao L, Du H, Wang Y, Yuan H (2014) Fe_3O_4 nanoparticles grown on graphene as advanced electrode materials for supercapacitors. J Power Sources 245:101–106

Xu L, Wang J (2012) Magnetic nanoscaled Fe_3O_4/CeO_2 composite as an efficient Fenton-like heterogeneous catalyst for degradation of 4-chlorophenol. Environ Sci Technol 46:10145–10153

Xu HY, Qi SY, Li Y, Zhao Y, Li JW (2013) Heterogeneous Fenton-like discoloration of Rhodamine B using natural schorl as catalyst: opti-mization by response surface methodology. Environ Sci Pollut Res 20:5764–5772

Yan Y, Jiang S, Zhang H (2016) Catalytic wet oxidation of phenol with Fe-ZSM-5 catalysts. RSC Adv 6:3850–3859

Yu L, Yang X, Ye Y, Wang D (2015) Efficient removal of atrazine in water with a Fe_3O_4/MWCNTs nanocomposite as a heterogeneous Fenton-like catalyst. RSC Adv 5:46059–46066

Zhang N, Zhao H, Zhang G, Chong S, Liu Y, Sun L, Chang H, Huang T (2017) Preparation of a magnetic N-Fe/AC catalyst for aqueous pharmaceutical treatment in heterogeneous sonication system. J Environ Manag 187:201–211

Zhang K, Wang JY, Zou JP, Cai WF, Zhang Q (2018) Low excitation of Raman D-band in [2+1] cycloaddition functionalized single-walled carbon nanotubes. Carbon 138:188–196

Zhou T, Feng K, Xiang W, Lv Y, Wu X, Mao J, He C (2018) Rapid decomposition of diclofenac in a magnetic field enhanced zerovalent iron/EDTA Fenton-like system. Chemosphere 193:968–977

Zgola-Grzeskowiak A, Grzeskowiak T (2011) Dispersive liquid-liquid microextraction. Trac-Trend Anal Chem 30:1382–1399

Zupanc M, Kosjek T, Petkovšek M, Dular M, Kompare B, Širok B, Blažeka Ž, Heath E (2013) Removal of pharmaceuticals from waste-water by biological processes, hydrodynamic cavitation and UV treatment. Ultrason Sonochem 20:1104–1112